# Clamped-Filament Elongation Model for Actin-Based Motors

Richard B. Dickinson* and Daniel L. Purich†
Department of *Chemical Engineering, University of Florida College of Engineering, and †Department of Biochemistry & Molecular Biology, University of Florida College of Medicine, Gainesville, Florida 32610-0245 USA

ABSTRACT Although actin-based motility drives cell crawling and intracellular locomotion of organelles and certain pathogens, the underlying mechanism of force generation remains a mystery. Recent experiments demonstrated that *Listeria* exhibit episodes of 5.4-nm stepwise motion corresponding to the periodicity of the actin filament subunits, and extremely small positional fluctuations during the intermittent pauses [S. C. Kuo and J. L. McGrath. 2000. *Nature.* 407:1026–1029]. These findings suggest that motile bacteria remain firmly bound to actin filament ends as they elongate, a behavior that appears to rule out previous models for actin-based motility. We propose and analyze a new mechanochemical model (called the "Lock, Load & Fire" mechanism) for force generation by means of affinity-modulated, clamped-filament elongation. During the *locking* step, the filament's terminal ATP-containing subunit binds tightly to a clamp situated on the surface of a motile object; in the *loading* step, actin·ATP monomer(s) bind to the filament end, an event that triggers the *firing* step, wherein ATP hydrolysis on the clamped subunit attenuates the filament's affinity for the clamp. This last step initiates translocation of the new ATP-containing terminus to the clamp, whereupon another cycle begins anew. This model explains how surface-tethered filaments can grow while exerting flexural or tensile force on the motile surface. Moreover, stochastic simulations of the model reproduce the signature motions of *Listeria*. This elongation motor, which we term actoclampin, exploits actin's intrinsic ATPase activity to provide a simple, high-fidelity enzymatic reaction cycle for force production that does not require elongating filaments to dissociate from the motile surface. This mechanism may operate whenever actin polymerization is called upon to generate the forces that drive cell crawling or intracellular organelle motility.

## INTRODUCTION

The cytoskeleton plays an indispensable role in cell motility (Bray, 1992; Stossel, 1993). In the case of actin-based motility, Peskin et al. (1993) offered the first model attempting to explain how polymerizing actin filaments might rectify the Brownian motion of an object to produce a unidirectional force. Their original "Brownian ratchet" model assumed the filaments were stiff, such that thermal fluctuations affected only the object being propelled. Because the thermal fluctuations of the motile object are too small to produce the observed motions, Mogilner and Oster (1996) later proposed the Elastic Brownian Ratchet model in which the thermal motions of the polymerizing filaments collectively produce a directed force. Both models require untethered filament ends at a surface for the free energy of monomer addition to generate a force.

Because the intracellular and in vitro motility of *Listeria monocytogenes* appears to reproduce all of the key features of actin-based motility in nonmuscle cells, this microorganism has become a widely studied model system. Through the use of a high-resolution, laser-tracking technique to study the detailed motions of *Listeria* in Cos7 cells, Kuo and McGrath (2000) reached the following conclusions: 1) motile bacteria move with extremely small Brownian fluctuations ($<0.1$ nm), suggesting a tight force balance between compressed and taut actin filaments in the actin tail tethered to the bacterial surface; and 2) in a manner reminiscent of molecular motors, *Listeria* trajectories exhibited 5.4-nm steps, corresponding to the subunit periodicity of actin filaments. Because filaments appeared to elongate at the bacterial surface while tethered, Kuo and McGrath argued against Brownian Ratchet models that required filament elongation and force generation by free filament ends that fluctuate away from the surface of the motile object (hereafter referred to as the motile surface). They also proposed that the forward force due to elongating flexed filaments is resisted by a few taut filaments, upon which bacteria appear to "slip" to reveal the 5.4-nm periodicity.

Based on the extremely small intermittent fluctuations observed between steps, Kuo and McGrath estimated a stiffness that would require a minimum force of 220 pN to displace the bacterium by 5.4 nm. These small fluctuations appeared to resume immediately after each 5.4-nm step, a finding that we take as evidence that the bond between the tethering apparatus (hereafter referred to as the "clamp") and the taut lagging filaments must have been stressed by a force of similar magnitude during each pause. Such forces are extremely large for noncovalent bonds, exceeding even the force needed to break avidin's highly affine bond for biotin ($K_d \sim 10^{-13}$ M) on a similar time scale (Merkel et al. 1999). Therefore, considering the large force apparently applied on the lagging filament, the observed $\sim$10-$s^{-1}$ "slip-rate" is unexpectedly slow. Moreover, if stepwise motion arises from rate-limiting advancement of a clamp on a lagging filament, and if such a large force were to accelerate clamp advancement, episodes of stepwise motion would not

*Submitted May 23, 2001; and accepted for publication September 28, 2001.*

Address reprint requests to Daniel L. Purich, Department of Biochemistry & Molecular Biology, Univ. Florida College of Medicine, Gainesville, FL 32610-0245. Tel. and Fax: 352-392-1546; E-mail: dlpurich@biochem.med.ufl.edu.



0006-3495/02/02/605/13 $2.00

endure. Despite this apparently strong filament-to-clamp bond, filaments under compression nonetheless grow rapidly, exhibiting elongation rates comparable to the diffusion-limited rate of monomer addition (Pollard et al., 2000). For filaments to remain tethered and for persistent stepwise motion to be revealed, the rate of clamp progression along a filament obviously cannot exceed the monomer addition rate. We take the fact that the clamp progresses at a rate close to, but not exceeding, the diffusion-limited monomer addition rate as evidence for an affinity-modulated mechanism, whereby new monomer addition somehow triggers a new cycle of release and advancement of the clamp. In such a mechanism, substantial energy would be required to attenuate the initially strong clamp-to-filament affinity and allow efficient clamp advancement and force generation on compressively flexed filaments.

Assuming filament elongation generates the force driving actin-based motility, then spontaneous, irreversible, and rapid filament growth requires the free energy change for monomer addition and clamp advancement to exceed the work needed to advance the clamp against an opposing force. The free energy change upon monomer addition alone is $-kT\ \ln([A]/[A]_{(+)critical})$, where $k$ is Boltzmann's constant, $T$ is the absolute temperature, [A] is the actin monomer concentration, and $[A]_{(+)critical}$ is the critical actin concentration of the (+) end. In previous actin-based motility models, large energy changes (e.g., 4.6–6.2 kT per monomer based on 10–50 $\mu$M (Mogilner and Oster, 1996) and 14 kT per monomer (Noireaux et al., 2000)) were assumed for calculating the substantial predicted forces. Because most of the intracellular unpolymerized actin is sequestered by thymosin-$\beta_4$, however, the free actin·ATP is only 3–10 $\times$ $[A]_{(+)critical}$ (Stossel, 1993); the resultant 1–2 kT per monomer could only sustain filament growth against forces of no more than 1.5–3.5 pN.

In myosin-based motility, ATP hydrolysis plays a central role in the mechanochemistry of force generation, and the same is true for dynein- and kinesin-based motility (Khan and Sheetz, 1997; Scholey et al., 1985). Actin filaments serve as a passive scaffold to and from which myosin attaches and detaches (Rayment et al., 1996), and microtubules do the same for dynein and kinesin motors. Even so, actin-bound ATP and tubulin-bound GTP hydrolyze during actin filament and microtubule self-assembly (MacNeal and Purich, 1978; Stossel, 1993). If the free energy of actin-bound ATP hydrolysis could be harnessed for work, 20 kT per monomer would be immediately available, assuming intracellular [ATP]/[ADP] of 10 and $[P_i]$ at 2 mM. Complete transduction of this chemical-bond energy into work could sustain a force of nearly 32 pN per filament. Cooke (1975a,b) demonstrated that hydrolysis is not required for monomer addition, because p(NH)ppA, a nonhydrolyzable ATP analog, supports filament assembly with little change in the critical concentration. It is known, however, that ATP hydrolysis is required for opposite-end filament assembly/disassembly ("treadmilling") by modifying the plus- and minus-end critical concentrations (Wegner and Engel, 1975). Because $[A]_{(-)critical}$ is approximately 10 $\times$ $[A]_{(+)critical}$ (Wegner, 1982), this difference in affinity requires only 2.3 kT, or ~10% of the total energy available from ATP hydrolysis.

These observations raise important new questions: How can filaments continue to elongate, while remaining strongly tethered to the surface? If tethering limits the forward motion, as suggested by Kuo and McGrath (2000), what advantage is gained by such a strong binding interaction between filaments and bacterial surface? Can a single growth rule explain rapid elongation of tethered filaments under either a strong tensile force (for taut filaments) or a strong compressive force (for flexed filaments)? How might an ensemble of elongating filaments lead to the signature stepwise motion with extremely small fluctuations during intermittent pauses? Finally, beyond the increment of energy required for treadmilling, what becomes of the remaining 90% of energy released during hydrolysis of filament-bound actin·ATP?

To address these and related issues, we propose a novel clamped-filament elongation mechanism that links force generation to affinity-modulated clamp interactions relying on the free energy of filament-bound ATP hydrolysis. In this cyclic process, a clamp remains locked onto an ATP-containing filament subunit until loading of new actin·ATP monomer(s) triggers ATP hydrolysis on the clamped subunit. The energy of ATP hydrolysis is transduced into a conformational change that attenuates filament affinity for the clamp, thereby allowing filament translocation and relocking of the clamp onto newly added ATP-containing subunits at or near the filament terminus. The model predicts force generation by surface-tethered, elongating filaments, even while under an opposing force, in a manner that reproduces the stepwise motion of *Listeria*. To our knowledge, this model is the first biophysical description of a molecular motor coupled directly to ATP hydrolysis during filament elongation.

## MODEL DESCRIPTION

### Clamped-filament growth

We have developed a model to explain how filaments can elongate while remaining strongly tethered to the motile surface, and how filament growth can generate a motile force. Shown in Fig. 1 is our model for a surface-bound, affinity-modulated clamp motor that is mechanochemically coupled to ATP hydrolysis during filament elongation. We refer to this mechanism as the "Lock, Load, & Fire" model, because it entails: *locking* of a surface-bound clamp onto the terminal actin·ATP subunit on the actin filament; *loading* of new actin·ATP monomers onto the terminus; and *firing* (i.e., hydrolysis) of ATP in the clamped subunit(s) to attenuate clamp affinity for the filament. This last step initiates clamp

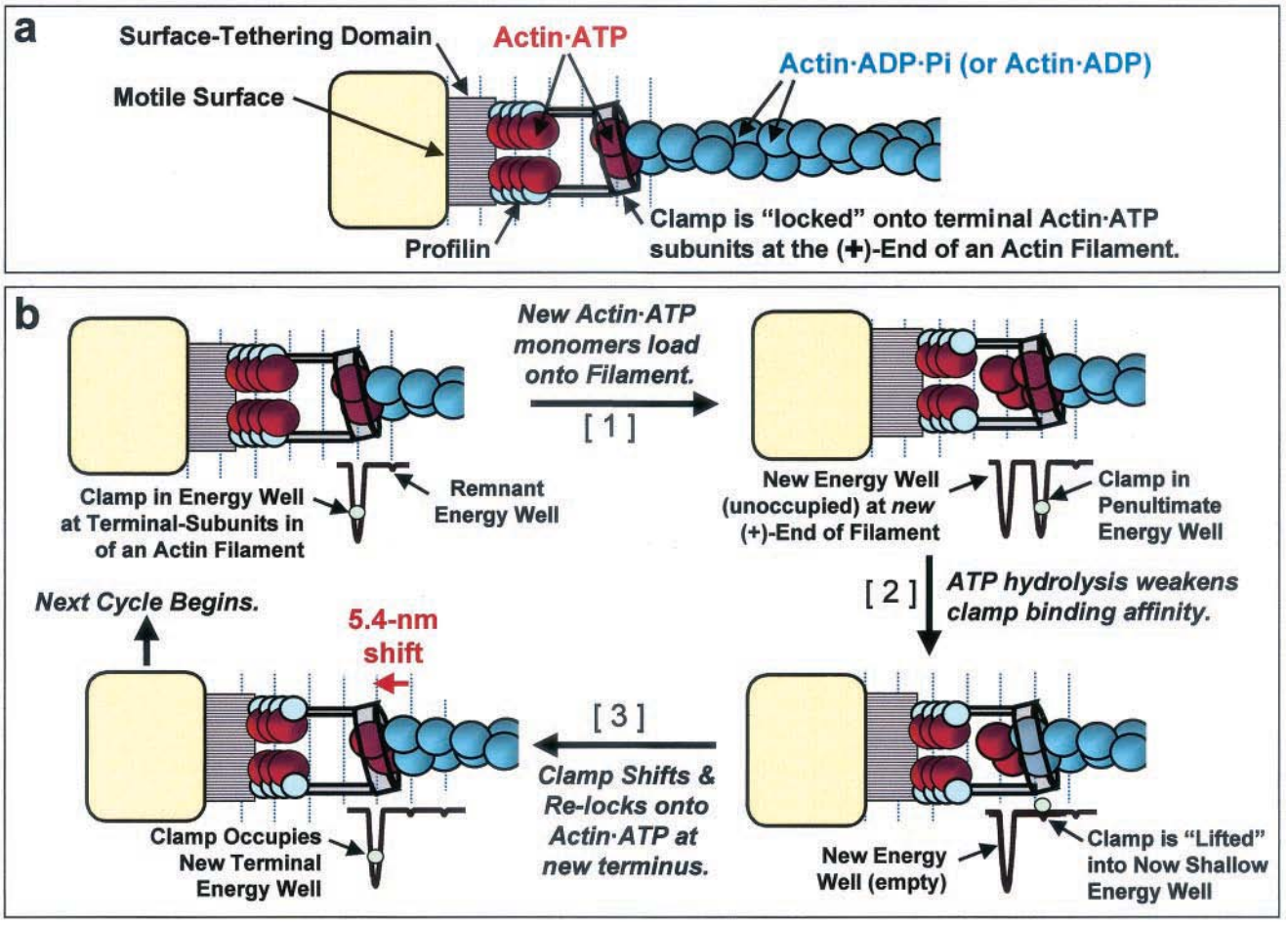


FIGURE 1 The Lock, Load & Fire model for a clamped-filament elongation motor. (*a*) Essential features are a surface-tethering domain and an affinity-modulated clamp. The role of the other components is specified in the text. This diagram illustrates the Locking (or high-affinity binding) of the clamp onto ATP-containing subunits at the filament end. [Note: Although not explicitly treated in this model, profilin (*light blue circles*) is likely to facilitate monomer addition by concentrating actin·ATP complex within the polymerization zone (see Discussion).] (*b*) The reaction begins with a clamped filament, the energy status of which is schematically represented by a green circle in the deep potential energy well situated immediately below the terminal actin·ATP (red subunits). Other shallow energy wells, located at 5.4-nm intervals along the filament, correspond to the greatly attenuated clamp affinity for actin·ADP·Pi or actin·ADP (both shown as blue subunits) within the filament. Each cycle of filament growth includes: 1) Loading of new ATP-containing monomers onto the filament end, a process that is schematically represented by the two additional red monomers and the unoccupied deep potential energy well positioned immediately below them; 2) Firing, wherein ATP hydrolysis attenuates clamp-binding affinity, as indicated by the conversion of a deep energy well to a shallow energy well; 3) Shifting and relocking, which includes the diffusive translocation and subsequent binding of the new filament end to the clamp (now shown as the green circle in the deep, terminal potential energy well).

translocation and relocking onto terminal ATP-containing subunits, whereupon another three-step cycle begins anew. In Fig. 1, the high-affinity and low-affinity binding sites are represented by deep and shallow potential energy wells, respectively. The mean total time required for one cycle, in which the clamp advances 5.4 nm, is therefore the time $T_m$ required for addition and ATP hydrolysis on two monomers, plus the mean time $\tau$ required for shifting and relocking onto the new terminus. (See Table 1 for definitions of symbols and parameters.) Growing filaments remain continuously tethered to the motile surface, and the energy of penultimate ATP hydrolysis enables essential conformational changes that attenuate clamp-to-filament binding energy. When the opposite ends of the filament are firmly immobilized in a cross-linked filament network (e.g., the "rocket" tail of motile *Listeria*), filament elongation will increase filament flexural force on the motile surface (Fig. 2). This simple growth rule for monomer addition, ATP hydrolysis, and clamp/filament translocation defines a repetitive enzymatic cycle of clamped-filament elongation and force generation.

## Force generation

For actin polymerization to generate a force, elongation must proceed even when the filament exerts a substantial

**TABLE 1 Definition of symbols and parameters**

| Symbol | Parameters |
|---|---|
| [A] | Actin monomer concentration |
| $[A]_{critical}$ | Macroscopic critical actin monomer concentration |
| $[A]_{(+)critical}$ | Microscopic critical actin monomer concentration for plus end |
| $[A]_{(-)critical}$ | Microscopic critical actin monomer concentration for minus end |
| $b$ | Diameter of actin filament |
| $d$ | Subunit spacing of an actin filament (5.4 nm) |
| $D_f$ | Filament diffusivity |
| $D_s$ | Diffusivity of motile surface |
| $F$ | Force on filament end |
| $F_{drag}$ | Drag force on motile surface |
| $k$ | Boltzmann's constant |
| $L$ | "Tube length" of actin filament |
| $n_T$ | Instantaneous number of filaments under tension |
| $N$ | Number of filaments tethered to motile surface |
| $R$ | Radius of curvature of tail-generating region on *Listeria* |
| $T$ | Absolute temperature |
| $T_m$ | Combined mean time for monomer-loading and ATP-hydrolysis steps |
| $v_s$ | Instantaneous velocity of motile surface |
| $W$ | Work required to shift filament end a distance of 5.4 nm |
| $z$ | Position variable for filament end during clamp shift |
| $z_0$ | Equilibrium position for filament end |
| $z_1$ | Position of filament end at instant of clamp dissociation |
| $z_s$ | Position of motile surface |
| $\delta_f$ | Coefficient of drag on filament |
| $\eta$ | Viscosity of fluid between filaments |
| $\kappa$ | Stiffness of filament under compression |
| $\kappa_T$ | Stiffness of filament under tension |
| $\lambda_p$ | Persistence length of actin filament |
| $\tau$ | Mean time for filament to shift one subunit following clamp dissociation |
| $\tau_{rel}$ | Relaxation time for position fluctuations of motile surface between shifts |
| $\xi$ | Mean spacing between filaments near motile surface |

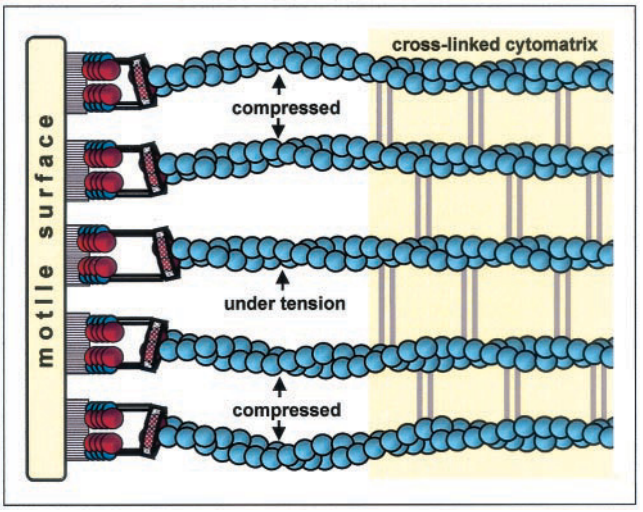


FIGURE 2 Illustration of typical filament states of an ensemble of elongating clamped filaments, with opposite ends anchored within a cross-linked network. Because filaments elongate independently, they exist in various states of monomer loading, elongation, compression, and tension. Each three-step elongation cycle increases the compressive force of the leading flexed filaments onto the motile surface, or relieves tension on taut lagging filaments. The motile surface advances when a force imbalance occurs, often resulting in discrete steps when the most lagging filament advances.

flexural force on the surface. In this respect, each cycle of new monomer addition and translocation performs mechanical work (i.e., a force acting through a distance). In our model, ATP hydrolysis drives this process by creating an energy difference between the clamp bound to penultimate actin·ADP versus the clamp bound to terminal actin·ATP. The rate of clamp translocation is determined by the energy landscape over the 5.4-nm distance between the two sites. Lacking the details of this landscape, a simple, self-consistent treatment is to assume a flat energy landscape between the shallow energy well (weak- or nonbinding) at the hydrolyzed site and an infinitely deep well (irreversible binding) at the adjacent nonhydrolyzed site. The transition in clamp position between the two wells is treated as one-dimensional diffusion of the free filament end (with diffusivity, $D_f$) over the 5.4-nm distance $d$ to fall immediately and irreversibly into the deep energy well. Depending on whether the filament is tense or flexed, this diffusion is either facilitated by the tensile force on a taut filament or opposed by the flexural force on a compressed filament. The time required for this displacement can be calculated as the mean time for the filament end to diffuse on the domain $z_1 \le z < z_1 + d$, starting at $z_1$ and reaching its instantaneous rebinding site at $z_1 + d$. We assumed a Hookean force–distance relationship, $F(z) = -\kappa(z - z_0)$, where $\kappa$ and $z_0$ are the stiffness and equilibrium position, respectively. By constraining the filament to move on a flat energy landscape only in the $z$-direction between $z_1$ and $z_1 + d$, we avoid making assumptions about the unknown details of intermolecular forces between the filament and the clamp. Our assumption of a reflective barrier at $z_1$ requires a pawl-like effect preventing the clamp from retreating toward subunits more distal from the filament terminus; such an effect could simply be created sterically by added monomers terminal to clamp, thereby preventing filament backsliding. For a compressed filament, the mean time $\tau$ for the filament to shift this distance under the compressive force $F(z)$ from the position $z_1$ to the perfect sink at $z_1 + d$ is shown in the Appendix to be

$$\tau = \frac{1}{D_f}\int_{z_1}^{z_1+d} dx e^{\kappa(x-z_0)^2/2kT}\int_{z_1}^{x} dy e^{-\kappa(y-z_0)^2/2kT}$$

$$= \frac{kT}{\kappa D_f}\sqrt{\pi}\int_{x_0}^{x_1} dx e^{x^2}(\mathrm{erf}[x] - \mathrm{erf}[x_0]), \qquad (1)$$

where $x_0 \equiv \sqrt{\kappa/2kT}(z_1 - z_0)$ and $x_1 \equiv \sqrt{\kappa/2kT}(z_1 + d - z_0)$. The more general treatment of a filament under either

tension or compression (or the transition between these two states) is presented in the Appendix.

Irreversible binding at $z_1 + d$ assumes that the difference between the binding energies of the clamp on the ADP- versus ATP-subunits (estimated to be up to 39 kT from the available free energy of hydrolysis of two subunits) is much larger than the work of clamp translocation. As shown in the Results section, we predict appreciable filament elongation rates up to ~12 pN of opposing force, corresponding to a maximal clamp-translocation work of about 16 kT. Because this maximal work is much less than the 39 kT of energy available from ATP hydrolysis, it is unnecessary to treat the clamp-translocation reaction as reversible; therefore, no explicit accounting for the energy of ATP hydrolysis is required.

## Stochastic simulations

To determine whether our model can faithfully generate the signature stepwise progression and small fluctuations reported by Kuo and McGrath (2000), we simulated the stochastic motion of a motile surface by accounting for the elastic and viscous forces associated with $N$ independent tethered filaments acting in parallel. As illustrated in Fig. 2, each filament $i$ was assumed to experience its own degree of compression/tension, depending on its hypothetical equilibrium end position, $z_{0,i}$, relative to the position $z_s$ of the motile surface. This Hookean spring force is given by

$$F_i = \begin{cases} -\kappa_T(z_{0,i} - z_s) & z_s \geq z_{0,i} \\ -\kappa(z_{0,i} - z_s) & z_s \geq z_{0,i} \end{cases} \quad (2)$$

where $\kappa_T$ and $\kappa$ are the filament stiffnesses under tension or compression, respectively. The clamp advancement corresponded to a shift in $z_{0,i}$ by a distance $d$ and was assumed to occur with a uniform probability per unit time, $1/(T_m + \tau)$, where $\tau$ was calculated from Eq. 1, using updated instantaneous values of $z_s$ and $z_{0,i}$. Although this treatment combines the sequential events of monomer addition, hydrolysis, and shifting of the clamp position into a single event, such an assumption only affects the waiting-time distribution between clamp translocations, not the mean time. A more detailed treatment, which must await experimental determination of the sequential steps and rate constants involved in monomer addition and induced hydrolysis, is beyond the immediate scope of this treatment.

Ignoring other viscous resistance (see Discussion), we only account for the viscous drag of the individual tethered filaments (see Discussion), each contributing a coefficient of drag, $\delta_f = kT/D_f$. We did not account for other contributions to viscous drag on the motile surface, which would require specifying unknown geometric details. Assuming that inertia of the motile surface is negligible compared to viscous forces, the motion of the motile surface can be described by the stochastic differential equation,

$$dz_s = v_s dt + \sqrt{2D_s}\, dW_t, \quad (3)$$

where $v_s = (1/N\delta_f) \sum_{i=1}^{N} F_i$ is the instantaneous deterministic velocity of the motile surface, $D_s = kT/N\delta_f = D_f/N$ is its effective diffusivity, and $dW_t$ is an increment in the Wiener process ($\langle dW_t \rangle = 0$, $\langle dW_t^2 \rangle = dt$). Eq. 3 was numerically integrated using the Euler algorithm (Gardiner, 1985) with a time increment, $\Delta t$, chosen by considering the characteristic relaxation time of the motile surface, $\tau_{rel} = N\delta_f/[n_T\kappa_T + (N - n_T)\kappa]$, where $n_T$ is the instantaneous number of filaments under tension. For the simulations shown here, the time increment was chosen as about one-tenth of the relaxation time for a single trailing filament, or 0.5 $\mu$s for 80 filaments. $dW$ was simulated using MATLAB's normally distributed psuedorandom number generator (Mathworks, Inc., Natick, MA). Increases in $z_{0,i}$ were made when MATLAB's routine for uniform pseudorandom number generation on the interval [0, 1] successfully yielded values less than $\Delta t/(T_m + \tau)$. The initial equilibrium positions of filament ends were randomly distributed over a 60-nm range, and the initial value of $z_s$ in the simulation was taken as the initial mechanical equilibrium position (where $\sum_{i=1}^{N} F_i = 0$) of this distribution. A histogram of the filament strain distribution ($z_{0,i} - z_s$) was tracked over time and found to evolve to an apparent steady-state distribution within a simulation time of several $T_m$. This distribution quickly stabilized because elongation rates of leading filaments began to stall under larger compression, and forward progression was limited by a few taut lagging filaments. It should be evident from Eq. 3 that the motion of the motile surface, resulting from the collective action of the ensemble of independent filaments, need not progress only by 5.4-nm steps when clamps on individual filaments translocate. In fact, clamp translocation on compressed filaments has only a small effect on motile-surface displacement. The motile surface advances by 5.4-nm steps only when the clamp on a single taut filament translocates, whereby the mechanical equilibrium position shifts by approximately 5.4 nm. When more than one filament is under tension, clamp translocation on filaments under tension results in smaller steps (see Results and Discussion).

## Parameter estimation

The key model parameters necessary in the model are $T_m$, $D_f$, $\kappa$, and $\kappa_T$. $D_f$ and $\kappa$ were estimated from statistical mechanical theory for semiflexible chains in semidilute solutions. A semiflexible actin filament segment of length $L$ can be approximated as a Hookean spring with longitudinal stiffness $\kappa = kT\lambda_p^2/L^4$ where $\lambda_p$ is the filament persistence length (Isambert and Maggs, 1996). Near the motile surface, where filament crowding is expected to be important, $L$

represents the tube length, defined as the characteristic distance between collisions of a filament with neighboring filaments. This parameter can be estimated from the mean spacing between filaments $\xi$, as $L \approx \xi^{4/5}\lambda_p^{1/5}$ (Isambert and Maggs, 1996). Unless otherwise noted, we estimate $\lambda_p = 15$ $\mu$m (Gittes et al., 1993) and $\xi = 100$ nm (assuming roughly 100 filaments crowded behind a motile bacterium's hemispherical pole of radius $R = 400$ nm and surface area $2\pi R^2 = 10^6$ nm$^2$), to calculate values of $L = 270$ nm and $\kappa = 0.17$ pN/nm. Note that thermal fluctuations reduce the filament's equilibrium length from the full length to a mean square end-to-end distance of $2\lambda_p[L - \lambda_p(1 - e^{-L/\lambda_p})]$ (Doi and Edwards, 1986). For parameters used above, the root-mean-square end-to-end distance is less than 1 nm away from its full length; therefore strain under tension can be assumed entirely due to stretching of the filament itself. We use an experimental value for the stretch stiffness $\kappa_T = 60$ pN/nm (Higuchi et al., 1995). The diffusivity of the filament segment is approximated by the rigid rod diffusivity, $D_f = kT\ln(L/b)/(4\pi\eta L) \approx 4 \times 10^6$ nm$^2$/s (Götter et al., 1996) where the filament diameter $b$ is taken as 7 nm (Janmey et al., 1990), and the interstitial fluid viscosity $\eta$ is taken as that of water ($10^{-9}$ pN-s/nm$^2$). Our assumption of constant parameters, $D_f$ and $\kappa$, requires that the cross-linked actin network that anchors filament ends distal to the motile surface advances continuously with $z_s$, such that the tube length used to estimate these parameters remains constant.

As shown under Results, the mean relocking time $\tau$ after firing of uncompressed filaments is predicted to be much shorter than typical experimentally observed times required for tethered filaments to elongate by 5.4 nm. Consequently, the model predicts that filament elongation must be rate-limited by the monomer-addition and ATP-hydrolysis steps, such that the motile surface progresses at an average rate approximately equal to $d/T_m$. Elongation rates during actin-based motility typically range from ~0.05 to 1 $\mu$m/s (Stossel 1993; Southwick and Purich, 1994), setting the range of $T_m$ values from 0.1 s down to 0.005 s.

## RESULTS

### Force effects on elongation rate

The mean time for a clamp translocation to occur (called the mean relocking time, $\tau$) as a function of applied force preceding the shift is plotted in Fig. 3 *A*. The results are shown for various values of the mean filament spacing, $\xi$, which determines the effective filament diffusivity and compressive stiffness. It can be shown by asymptotic analysis of Eq. 1 that, for larger compressive forces $\kappa(z_1 - z_0) \gg \sqrt{\kappa kT}$, $\tau$ increases with an approximate exponential dependence on the translocation work, $W = \kappa[(z_1 - z_0)d + \frac{1}{2}d^2]$, which is approximately equal to $\kappa(z_1 - z_0)d$, when $(z_1 - z_0) \gg d$. Therefore, $W$ is effectively the transition-state energy for the clamp-translocation event. Unless the compressive force is greater than ~6–8 pN, the mean relocking time $\tau$ is predicted to be much smaller than the typical observed times required for filaments to elongate 5.4 nm during actin-based motility. Consequently, if velocities in actin-based motility are limited by the elongation rates of lagging filaments (those not under strong compression), a self-consistent conclusion is that the mean speed of the motile surface is limited primarily by monomer addition/ATP-hydrolysis (i.e., by $T_m$ rather than by $\tau$). These times, and the total mean time $\tau + T_m$ for a complete cycle of loading, firing, and relocking, are plotted in Fig. 3 *A*. Here, we have used an intermediate value of $T_m$ (i.e., 0.027 s) based on an assumed maximal elongation rate $d/T_m$ of 200 nm/s. The force-dependent elongation rates (corresponding to the mean shift times in Fig. 3 *A*) are shown in Fig. 3 *B*. Long shift times at higher forces have the effect of stalling elongation. Over the range of filament spacing values shown (i.e., 50 nm $< \xi <$ 125 nm), filament growth is predicted to stall only when the compressive force greatly exceeds ~8 pN. The model predicts a force-independent growth rate for smaller opposing forces, where growth is limited only by $T_m$. The clamped-filament elongation rate should remain unimpeded for significant opposing forces, thereby allowing the filament to exert up to several pN of flexural force onto the motile surface.

### Simulation of actin-based motility

The signature stepwise progression and small fluctuations reported by Kuo and McGrath (2000) have been faithfully reproduced in our simulations of a motile surface propelled by a large number of filaments that obey the Lock, Load, & Fire mechanism. Simulated trajectories of the motile surface are shown in Fig. 4 *A* for a system of 80 clamped filaments and maximal filament growth rates of 50 and 200 nm/s. These trajectories represent a short time interval of a longer trajectory, taken after the steady-state distribution of filament equilibrium lengths relative to $z_s$ was established. As a consequence of the reduced filament growth rate under large compressive forces and the lagging filaments limiting the velocity, the mean velocity of the surface was ~80–90% of the maximal filament growth rate, $d/T_m$.

Consistent with the experimental observations by Kuo and McGrath (2000), the simulated motion exhibited stepwise progression with small fluctuations during intermittent pauses (Fig. 4 *A*). When the long-time trajectories (10 s of total simulated time after reaching steady state) were analyzed in terms of their pair-wise displacements, we obtained a distribution (Fig. 4 *B*) displaying major peaks equally spaced at 5.4-nm intervals. The power spectrum of this pairwise frequency distribution (Fig. 4 *C*) exhibited a major peak situated at 0.18 nm$^{-1}$ (the reciprocal of the 5.4-nm periodicity); additional peaks are spaced at intervals of $\sim n/5.4$ nm$^{-1}$ (where $n = 1, 2, 3, \ldots$). This simulation therefore shows the same strong 0.18-nm$^{-1}$ peak and a

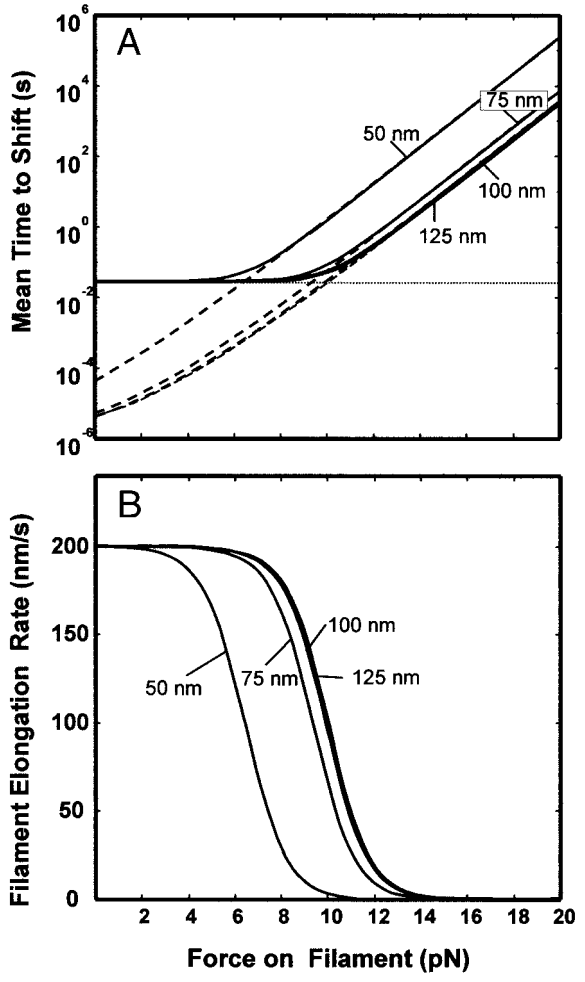


FIGURE 3 Predicted motile properties of a motor operating by the Lock, Load, & Fire mechanism. (*A*) Plot of the mean time and (*B*) resultant growth rates for one filament-elongation cycle versus applied force. Curves are shown for various values of the mean filament spacing $\xi$, which influences the effective filament diffusivity and stiffness. The total mean time (*solid blue lines*) for monomer addition (loading), ATP hydrolysis (firing), and clamp translocation (relocking) is the sum of the force-dependent mean relocking time $\tau$ (*solid red lines*) and the force-independent mean time to load and fire $T_m$ (*horizontal dashed red line*).

smaller 0.36-nm$^{-1}$ peak observed by Kuo and McGrath (2000), who noted that smaller peaks at higher frequencies in the experiments would have been obscured by measurement noise. The location of the peaks in the power spectrum can be understood in terms of the steps resulting from various states of filament compression/tension. The 5.4-nm steps correspond to the release and relocking of a single lagging filament under tension, with the other filaments remaining under compression throughout the step. Additional peaks in the power spectrum correspond to smaller 5.4/*n*-nm fractional step sizes, which resulted from a variable number of trailing filaments under tension. For example, a discrete 2.7-nm step occurred when one of only two tense filaments shifted. During the simulated time evolution of filament growth, the number of filaments under tension varied slowly; extended episodes occurred where only one or two filaments were tense, and episodes with three or more tense filaments were rare. As indicated by the spectra in Fig. 4 *C*, doubling the number of filaments increased the weight of the higher frequency peaks. However, simulations consistently showed that the filament number did not significantly affect the overall mean speed of the motile surface, as expected when the speed is limited only by clamp translocation rate of the most lagging filament(s).

Because all filaments remain tethered to the surface, the model also predicts that the strong compressive force exerted by multiple flexed filaments balances the correspondingly large tension on a few lagging filaments. The total stiffness of motile surface between steps was $\kappa_{eff} = n_T\kappa_T + (N - n_T)\kappa$, which resulted in small positional fluctuations $(kT/\kappa_{eff})^{1/2} \sim 0.1–0.2$ nm, depending on the instantaneous number of trailing filaments. The magnitude of these fluctuations was consistent with the very small fluctuations observed with motile *Listeria* (Kuo and McGrath, 2000).

Simulations were repeated for several different filament numbers and for different values of the filament stiffness and diffusivity. These parameters did not appreciably influence the mean speed of the motile surface, which was primarily determined by $d/T_m$. Whenever $\kappa_T \gg \kappa$, stepwise motion with 5.4-nm increments and small fluctuations during intermittent pauses consistently appeared.

## DISCUSSION

The Lock, Load, & Fire mechanism for actin-based motility treats the force-producing step as a consequence of an affinity-modulating ATP-hydrolysis reaction linked directly to filament elongation. The scheme explains how tethered filaments can continue to elongate unhindered while under moderate compressive forces (less than ~8 pN/filament) and still remain tethered while elongating under a large tensile force. Our model-based simulations faithfully predict both the signature step-wise motions and the very small positional fluctuations observed by Kuo and McGrath (2000). We therefore suggest that this model, or some closely related variant, describes the force-producing process in actin-based motility.

Beyond those properties already considered, our model also predicts other significant features of a clamped-filament elongation motor. First, except for large opposing forces (>6–10 pN/filament), the motility rate should be limited only by the composite rate constant for monomer loading and ATP hydrolysis (loading and firing); it is the latter process that relieves the tension exerted on the lagging filament(s). Second, the model predicts that filament elongation should stall only when large compressive forces are exerted on the filament. Third, the model anticipates a weak dependence, if any, of the motility rate on the number of filaments propelling the motile surface. Fourth, the model

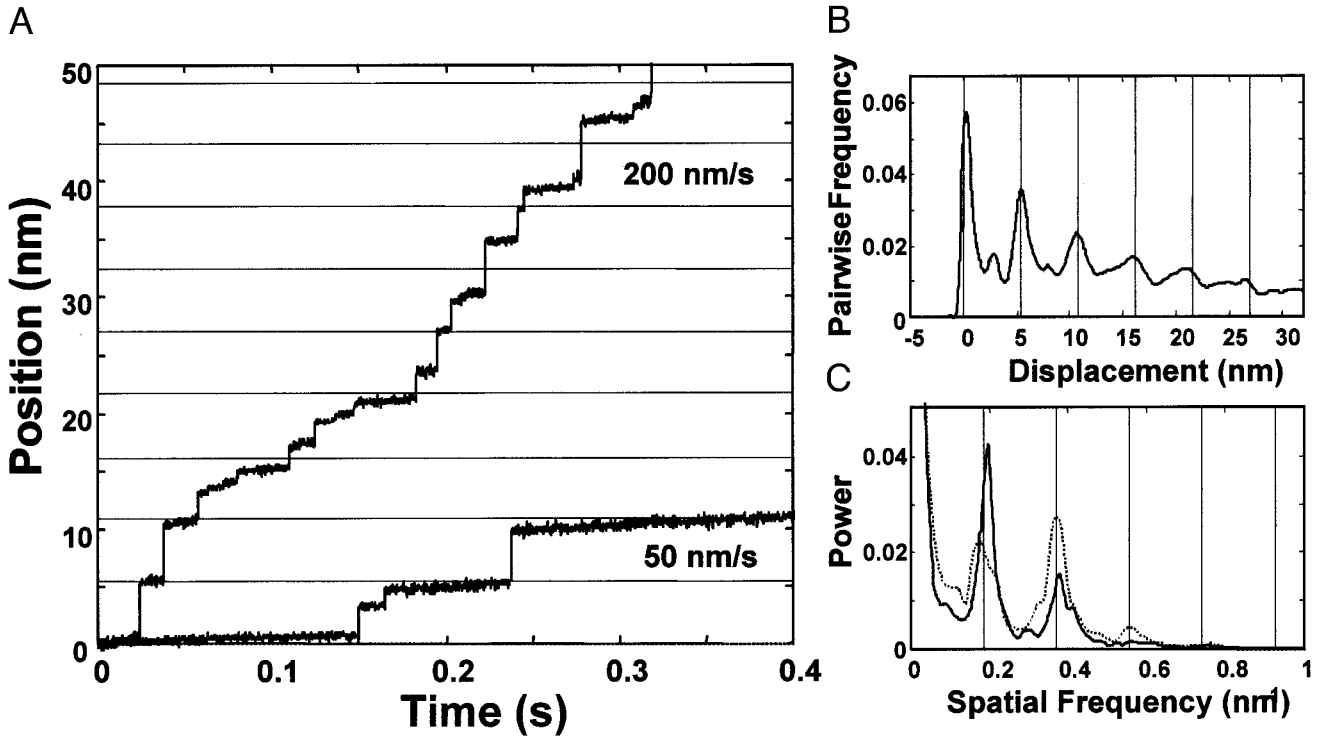


FIGURE 4 (*A*) Simulated trajectories exhibiting stepwise motions with small positional fluctuations during intermittent pauses for two different maximal filament growth rates, $d/T_m$ = 50 nm/s and 200 nm/s. The red lines show 5.4-nm steps corresponding to the subunit periodicity of actin filaments. (*B*) Distribution of pairwise displacements from a 10-s simulation ($d/T_m$ = 200 nm/s). The major peaks are indicative of pauses spaced predominantly at 5.4-nm intervals, reflecting the monomer-sized steps taken as a single lagging filament shifts by one register. (*C*) Power spectrum of the pairwise frequency distribution. Note the major peaks of decreasing magnitude spaced at 0.18-nm$^{-1}$ intervals. These peaks measure the periodicity in the pairwise frequency distribution that resulted from discrete 5.4/*n*-nm steps, where $n = 1, 2, 3$. Peaks corresponding to $n > 2$ resulted from episodes where $n$ lagging filaments under tension balanced the compressive forces of the other leading filaments. When a lagging filament is released from a clamp, its tension is transferred to the remaining $n - 1$ filaments, resulting in a 5.4/*n*-nm step. Also shown is a spectrum for a simulation carried out with 160 filaments for the same parameter values (*dashed line*), exhibiting larger peaks at higher spatial frequencies due to an increased number of fractional steps when more filaments act on the surface. Other than its effect on the step-size distribution, the filament number did not significantly affect the long-time mean speed of the motile surface, which was limited by the advancement of the most-lagging filament(s).

simulations could reproduce experimentally consistent motile behavior without invoking the viscous properties of the surrounding medium or the mechanical properties of the surrounding actin network, beyond those factors affecting filament orientation, effective stiffness, and filament-end diffusivity. Supporting these predictions is the consistent finding that *Shigella* moves as fast as *Listeria*, despite the fact that *Shigella* is nearly twice as large and contains fewer filaments in its rocket tail (Zeile et al., 1996; Suzuki et al., 1996). Also, the motility rates of both microorganisms does not appear to correlate with the viscosity of the surrounding medium, whether it is the cytoplasm of intact cells or in diluted cell extracts.

Several simplifying assumptions facilitated analysis of the clamped-filament growth model and allowed us to avoid specifying the details of the motile surface. For example, we have assumed a parallel array of filaments, consistent with the filament orientations observed within filipodia and in *Listeria* rocket tails (Sechi et al., 1997). Also, we expect tethered filaments to be swept into alignment by the strong action of the other filaments pushing the motile surface. We also chose not to account for any force-induced dissociation of filaments from the clamp, dissociation of the clamp from the motile surface, or breakage of filaments under tension, although we expect these effects to be small based on the experimentally observed persistent stepwise motion of *Listeria* (Kuo and McGrath, 2000). We also have not explicitly accounted for any filament binding interactions that may affect the assumed stiffness or mobility of filament segments in the neighborhood of the clamp/surface. In this respect, we recognize that other filament side-binding proteins (e.g., tropomyosin, cofilin, etc.) may modulate the filament's mechanical properties. We have also neglected viscous interactions beyond those of the tethered filaments, which avoids consideration of the hydrodynamic profile of the propelled object or specifying other viscous resistance to the motion. We estimate that the effective viscosity of the surrounding medium would have to be roughly ten times larger than the interstitial fluid viscosity for the drag on a propelled object (400-nm radius) to exceed the drag caused

by 80 tethered filaments. In any case, the magnitude of viscous drag only affects the relaxation time of positional fluctuations, without altering the key characteristics of the trajectories on a longer time scale (i.e., the magnitude of the fluctuations, the stepwise motion, and the mean velocity). Finally, as in previous biophysical models (Noireaux et al., 2000; Mogilner and Oster, 1996) of actin-based motility, we have taken an admittedly coarse-grained approach of estimating the stiffness and mobility of filaments from theories for semiflexible worm-like chains in semidilute solution, thus avoiding detailed modeling of filament dynamics and filament–filament interactions. Exclusion of these complications does not compromise the key conclusions of sustained filament elongation under a large force and step-wise motion with small fluctuations during intermittent pauses.

In our model, the energy of rapid ATP hydrolysis following monomer addition reduces the binding affinity of the clamp on the penultimate subunit, thereby creating a binding energy differential between the low-affinity penultimate binding site and the high-affinity terminal site. This energy differential is the thermodynamic driving force for irreversible shifting of the clamp to the new terminal end. The most straightforward way to model this process was to treat the shift as "diffusion" of the filament between the two clamp-binding sites. On an energy landscape of the clamp–filament interaction, binding-site dimensions were considered small compared to 5.4 nm. Moreover, lacking actual rate constants, we assumed that clamp dissociation from actin·ATP was negligibly slow (corresponding to an infinitely deep energy well) on the relevant time scale, whereas clamp dissociation from actin·ADP was assumed to be fast. Therefore, the energy of ATP hydrolysis is implicitly accounted for in the boundary conditions for the differential equation (Appendix) whose solution is shown in Eq. 1. The hydrolysis energy was taken to be large enough to convert a deep potential well into a shallow well at the penultimate site, and to make rebinding at the terminal site irreversible. In the absence of details of the energy landscape, our approach reasonably predicts the rate-dependence of clamp advancement on a filament under an opposing force.

We have not specified the precise step in the pathway from ATP hydrolysis to phosphate release where the clamp-binding affinity is attenuated. In principle, this could occur at one of at least three stages: conversion of filament-bound actin·ATP to form filament-bound actin·ADP·$P_i$; conversion of filament-bound actin·ATP to form filament-bound actin*·ADP·$P_i$ (where the * indicates stored conformational energy), followed by conversion to actin·ADP·$P_i$; and conversion of filament-bound actin·ADP·$P_i$ to form actin·ADP (with the release of phosphate). Recent studies on the crystal structure of actin·ADP complex suggest a model for how $P_i$-release after ATP hydrolysis may change the actin protein conformation and its dynamics during filament assembly (Otterbein et al., 2001). Because their structural studies were carried out with actin monomer, it remains to be determined if the same is true for actin units in a filament.

Our assumption that actin-bound ATP hydrolysis attenuates the affinity of filament-to-clamp interaction remains to be experimentally verified. Nevertheless, there is ample precedence in the cytoskeletal and signal-transduction literature for modulation of protein–protein binding affinity through hydrolysis of nucleoside 5′-triphosphates (Purich, 2001). For example, ATP hydrolysis attenuates actin monomer affinity for filament ends and binding interactions between adjacent subunits in an assembled filament (Pollard, 1986a,b; Pollard et al., 2000). In this case and in our model, the high-affinity state is the nucleoside 5′-triphosphate-containing subunit. A similar type of affinity modulation occurs in GTP-dependent microtubule assembly/disassembly, with tubulin·GDP exhibiting much lower affinity for microtubule ends than tubulin·GTP (Karr et al., 1979; Purich and Southwick, 1999). Finally, the regulatory action of many G-proteins is thought to be affinity modulated in a similar manner (Vale, 1996; Purich, 2001).

Treating the filament shift as a diffusion-limited process assumes that the work of the relocking step exceeds the energy of any peaks in the free energy landscape between the binding positions. If the energy of a transition barrier exceeds this work at some intermediate distance $\Delta < d$, then the energy barrier is predicted to increase with compression by $\kappa(z_1 - z_0 + \Delta)\Delta$, making $\tau$ scale with $\exp[\kappa(z_1 - z_0 + \Delta)\Delta/kT]$, rather than with $\exp[\kappa(z_1 - z_0 + d/2)d/kT]$. Consequently, as observed in studies of force-dependent bond breakage (Merkel et al., 1999), different exponential dependencies on force may arise at different regimes of compressive force. Such considerations await additional details about the energy landscape of clamp-to-filament interaction and its transitions. In any case, such variations to the model would not alter the prediction of an exponential dependence of the mean relocking time on the applied force.

Because we have neglected the viscous drag of the motile surface itself, no net work attends its translation, and the energy of ATP hydrolysis (beyond that needed for treadmilling) is ultimately dissipated as heat. This feature is neither unexpected nor unreasonable given the fact that, for example, the work required to translate a bacterium at a nominal speed of 200 nm/s is 5–6 orders of magnitude less than the energy released in ATP hydrolysis on 80 tethered filaments in the actin-rich rocket tail during the motion. In the absence of a significant resisting force, the energy of ATP hydrolysis is instead expended to establish tensegrity at the motile surface due to the force balance between leading and lagging filaments. However, by providing up to 8 pN per filament without stalling, ATP hydrolysis could yield far more than enough force than would be needed, for example, to drive a motile bacterium unimpeded through highly viscous regions within the cytoplasm. This feature may explain the smooth trajectories of *Listeria* in time-lapse video microscopy (Dabiri et al., 1990). How the energy of

ATP hydrolysis ultimately dissipates into heat depends on whether a filament is compressed or under tension. When under compression, the energy of hydrolysis drives the filament to reach a new state of greater flexure, such that the chemical energy is temporarily converted to mechanical energy. In contrast, when a filament is under tension, the hydrolysis-induced clamp release results in a sudden force imbalance between the flexural and tensile forces within the ensemble. This imbalance allows the motile surface to proceed in a forward motion that is resisted by the viscous drag of the other tethered filaments until the forces are again rebalanced. This action converts a portion of the accumulated mechanical energy of the flexed filaments into heat by viscous dissipation, leaving the rest to be lost as heat in later steps. Whenever elongation becomes uncoupled from clamp advancement, as would be expected in the case of in vitro actin polymerization, chemical-bond energy released during ATP hydrolysis will be dissipated directly as heat.

If the Lock, Load, & Fire mechanism is the main route for actin polymerization in living cells, then penultimate hydrolysis should make ADP the predominant nucleotide in actin filaments. A virtue of this affinity-modulated mechanism is that the clamp-to-filament bond is maintained throughout all steps in the motile process, even when actin·ATP monomers are scarce or unavailable. The phenomenon of penultimate hydrolysis was first observed with microtubules and served as the basis for boundary-stabilization during microtubule assembly/disassembly (Karr et al., 1979). In this case, newly added tubulin·GTP dimers induce hydrolysis of GTP on the penultimate tubulin dimers in a microtubule (Purich and Angelastro, 1994; Purich and Southwick, 1999; O'Brien et al., 1987). Although there is limited evidence concerning penultimate hydrolysis during actin filament assembly, Angelastro and Purich (1994) determined that the ATP and ADP content of actin filaments isolated intact from PC12 cells, neuroblastoma cells, rat embryonic dorsal root ganglion neurons, and their measurements were consistent with the presence of only a few actin·ATP molecules on the (+)ends of actin filaments. They suggested that new monomer addition somehow facilitates ATP hydrolysis on the neighboring or penultimate actin subunit of filaments assembling within cells. In the absence of affinity-modulated clamps, in vitro actin assembly is known to permit the accumulation of more actin·ATP molecules on the (+)ends. Because filament severing by gelsolin and related proteins should result in the formation of unclamped filaments, one cannot discount the likely accumulation of actin·ATP molecules on unclampled filament ends.

Our model effectively treats penultimate ATP hydrolysis as a fast first-order isomerization (actin·ATP $\rightarrow$ actin·ADP· $P_i$) that is triggered by addition of the new actin·ATP at the filament end. If the rate constant for ATP hydrolysis did not greatly exceed the rate constant for monomer addition, then hydrolysis would not occur strictly on penultimate subunits. This circumstance could lead to an accumulation of multiple actin·ATP subunits on the terminal side of the clamp, to the extent allowed by steric constraints. Provided that terminal actin·ATP subunits hydrolyze slowly relative to the rate of adding new monomers, the clamp will still tether the filament to the surface. However, two lines of evidence weigh against slower exponential ATP hydrolysis on subunits on the terminal side of the clamp: 1) clamp advancement proceeds at a rate comparable to the diffusion-limited monomer-addition rate, suggesting that the processes are coupled, such that monomer addition triggers prompt hydrolysis; and 2) uncoupled ATP-hydrolysis on subunits terminal with respect to the clamp position would be expected to occasionally result in step skipping, whereby the clamp shifts past a number of weak-binding actin·ADP subunits that have already undergone hydrolysis. The latter feature was not evident in trajectories of Kuo and McGrath (2000). In any case, our model can be readily extended to deal with the possibility of hydrolyzed subunits terminal to the clamp by accounting for the individual events of monomer addition and hydrolysis and clamp translocation over distances corresponding to steps over multiple subunits (i.e., 5.4 nm, 10.8 nm, 16.2 nm, etc.). Finally, one cannot exclude the possibility that the clamp's association with the filament end would lead to accelerated penultimate ATP hydrolysis, analogous to the 50–200-times enhancement of myosin ATPase activity in the presence of assembled actin filaments (Cooke, 1975a).

Recent investigations suggest that two related families of proteins may serve as building blocks for the affinity-modulated clamps proposed in our model. First, *Drosophila* Ena (Gertler et al., 1995) and mammalian vasodilator-stimulated phosphoprotein (VASP) (Bachmann et al., 1999) are the founding members of the Ena/VASP family that also includes Mena, Avena, RNB6, and the Ena/VASP-like protein known as Evl. These actin-regulatory proteins are found associated with actin filaments in focal adhesions and highly dynamic membrane regions undergoing filipodium formation, lamellipodium extension, and various forms of ruffling. The C-terminal EVH1 domain anchors VASP onto the motile surface of membrane-protrusion sites or at the trailing pole of motile intracellular pathogens such as *Listeria* (Niebuhr et al., 1997; Southwick and Purich, 1996), *Shigella* (Suzuki et al., 1996; Laine et al., 1997), and vaccinia (Zeile et al., 1998). The central proline-rich domains bind profilin and profilin·actin·ATP, which likely facilitates monomer loading in our proposed mechanism. The EVH2 domain, which is the likely filament-binding domain in our model, lacks any recognizable ATP-binding motif found in other motor proteins. Bachmann et al. (1999) found that human VASP contains an F-actin binding domain

(residues 259–276), which resembles the C-terminal region in the filament side-binding protein villin. Second, Wiscott–Aldrich sydrome protein (WASP) and its neuronal analog N-WASP are distantly related to the Ena/VASP family (Reinhard et al., 2001). N-WASP is known to be essential for *Shigella* (Mimuro et al., 2000) and vaccinia motility (Frischknecht et al., 1999). It is also significant that both WASP and N-WASP contain N-terminal EVH1 domains, centrally located proline-rich domains, and verprolin-homology regions and C-terminal cofilin homology domains. Like villin, cofilin is known to bind with high affinity to the surface of actin filaments, and the presence of a cofilin homology region in WASP and N-WASP suggests an attractive means for assembling an affinity-modulated clamp. Although it is too early to know how affinity-modulated clamps are assembled, the structural features of these actin-regulatory proteins provide promising hints about some of the essential binding interactions. We stress that other actin-regulatory proteins, beyond those described above, may also be involved in the active motor unit, and future studies must address the minimal components required for motor assembly and activity.

Clamped-filament growth is reminiscent of DNA polymerase processivity (Kuriyan and O'Donnell, 1993; Bloom et al., 1996), a kinetic phenomenon that improves polymerization efficiency by keeping a polymerase in contact with its biopolymer substrate throughout multiple catalytic rounds (McClure and Chow, 1980). Our proposed mechanism anticipates an initial clamp-loading step that generates the high-affinity interaction between the clamp and its elongating filament. The Arp2/3 complex may fulfill this role in at least two ways: first by nucleating new filaments, such that terminal subunit ATP hydrolysis is prevented, and second by loading ATP-containing nuclei onto empty clamps. *Listeria* ActA is known to activate Arp2/3-dependent actin nucleation, but further work is also needed to learn whether these nuclei contain actin·ATP and precisely how ActA–Arp2/3 binding might facilitate the insertion of polymerization nuclei in empty clamps. Recent investigations suggest that Arp2/3 complex must be supplied continuously to maintain actin-based motility (Pollard et al., 2000), and, by controlling the supply of polymerization nuclei, Arp2/3 may be a critical component for regulating the activity of our putative clamped-filament elongation motor.

In summary, our proposed model is consistent with published observations of actin-based motility and the properties of actin and known cytoskeletal proteins. The clamped-filament growth model involves force-generation by surface-tethered filaments and successfully predicts the small fluctuations and stepwise motions as the collective action of an ensemble of clamped filaments. In contrast to apparently similar motions of stepper-type molecular motors (e.g., myosin, dynein, and kinesin), this characteristic behavior arises from the forward force generated by the leading filaments after the release and translocation of a lagging filament on its clamp. To identify this putative motor complex, we offer the name *actoclampin*, a composite of two root words and a suffix: "acto-" (from actin, as in *acto*myosin) + "clamp" (meaning a clasping device used for strengthening flexible/moving objects and for securely fastening two or more components) + "in" (designating its protein origin). The actoclampin motor would be unique among known molecular motors in that hydrolysis of filament-bound actin·ATP is predicted to modulate the clamp binding strength to promote filament elongation and force production simultaneously.

## APPENDIX

In this Appendix, we derive the mean time for the filament end to shift a distance, $d$, to rebind to the clamp. The filament end is assumed to be subjected to a force, $F(z)$, and fluctuates in position with characteristic diffusivity, $D_f$. The Fokker–Planck equation for the probability density, $p(z, t|z', 0)$, is given by

$$\frac{\partial p(z, t|z', 0)}{\partial t} = -\frac{\partial}{\partial z}\left[\frac{D_f}{kT}F(z)p(z, t|z', 0) + D_f\frac{\partial p(z, t|z', 0)}{\partial z}\right], \quad \text{(A1)}$$

where $z$ is the filament end position at time $t$, and $z'$ is the position at time zero. The force on the filament end due to compression and tension is given by

$$F(z) = \begin{cases} -\kappa_T(z - z_0) & z < z_0 \\ -\kappa(z - z_0) & z \geq z_0 \end{cases}, \quad \text{(A2)}$$

where $z_0$ is the hypothetical equilibrium filament-end position. As shown in Gardiner (1985) the mean exit time $\tau$, from the interval $z_1 < z < z_1 + d$, is governed by the differential equation

$$\frac{D_f}{kT}F(z')\frac{d\tau}{dz'} + D_f\frac{d^2\tau}{dz'^2} = -1 \quad \text{(A3)}$$

with boundary conditions, $(d\tau/dz)|_{z_1} = 0$ and $\tau(z_1 + d) = 0$. The solution is

$$\tau = \frac{1}{D_f}\int_{z_1}^{z_1+d} dx\psi^{-1}(x)\int_{z_1}^{x} dy\psi(y), \quad \text{(A4)}$$

where

$$\psi(x) = \exp\left[\int_{z_1}^{x} dz\frac{F(z)}{kT}\right] = \begin{cases} \exp\left(\frac{\kappa_T(z_0 - z_1)^2}{2kT}\right)\exp\left(\frac{-\kappa(x - z_0)^2}{2kT}\right) & \text{for } z_1 \leq z_0 \leq x \\ \exp\left(\frac{\kappa_T(z_0 - z_1)^2}{2kT}\right)\exp\left(\frac{-\kappa_T(x - z_0)^2}{2kT}\right) & \text{for } z_1 \leq x < z_0 \\ \exp\left(\frac{\kappa(z_0 - z_1)^2}{2kT}\right)\exp\left(\frac{-\kappa(x - z_0)^2}{2kT}\right) & \text{for } z_0 < z_1. \end{cases} \quad \text{(A5)}$$

Carrying out the integrals yields

$$\tau = \frac{\sqrt{\pi}}{D_f}\begin{cases} \sigma^2 \int_{x_1}^{x_2} dx e^{x^2}(\mathrm{erf}[x] - \mathrm{erf}[x_1]) & \text{for} \quad z_1 \geq z_0 \\ \sigma_T^2 \int_{-x_2}^{-x_1} dx e^{x^2}(\mathrm{erf}[-x_1] - \mathrm{erf}[x]) & \text{for} \quad z_1 + d < z_0 \\ \sigma_T^2 \int_{0}^{-x_1} dx e^{x^2}(\mathrm{erf}[-x_1] - \mathrm{erf}[x]) & \\ \quad + \int_{0}^{x_2} dx e^{x^2}[\sigma_T \sigma\, \mathrm{erf}[-x_1] + \sigma^2 \mathrm{erf}[x]] & \text{for} \quad z_1 < z_0 < z_1 + d, \end{cases} \tag{A6}$$

where

$$\sigma \equiv \sqrt{\frac{kT}{\kappa}}, \quad \sigma_T \equiv \sqrt{\frac{kT}{\kappa_T}},$$

and the integral limits are given by

$$x_1 = \begin{cases} \dfrac{(z_1 - z_0)}{\sqrt{2}\sigma} & \text{for} \quad z_1 \geq z_0 \\ \dfrac{(z_1 - z_0)}{\sqrt{2}\sigma_T} & \text{for} \quad z_1 < z_0 \end{cases}$$

and

$$x_2 = \begin{cases} \dfrac{(z_1 - z_0 + d)}{\sqrt{2}\sigma} & \text{for} \quad z_1 + d \geq z_0 \\ \dfrac{(z_1 - z_0 + D)}{\sqrt{2}\sigma_T} & \text{for} \quad z_1 + d < z_0. \end{cases}$$

**Note Added in Proof:** After submitting our manuscript, we became aware of the report by Lindberg et al. (1981), who were probably the first to glimpse the actoclampin motor in electron micrographs of the leading edge of motile glial cells. They proposed that profilin·actin complex is the immediate precursor for filaments that assemble into membrane-associated "organizing units" during motility. Hajkova et al. (2000) also reported that covalently cross-linked profilin·actin (abbreviated: P×A) promptly arrests all actin-dependent motility upon microinjection into cultured cells. We take their observation of P×A-induced trapping of actin filaments on the peripheral membrane's inner surface as an indication that the actoclampin motor advances and locks onto P×A, thereby arresting motility by sterically blocking filament elongation. If P×A proves to be a potent substoichiometric motility inhibitor, such an observation would essentially verify our assumption that each force-producing filament is bound to the motile surface by means of an affinity-modulated clamp.

This investigation was supported in part by grants from the University of Florida's Biomedical Engineering Program and Office of Research and Graduate Education.

We also thank our colleagues Brian Burgess, Frederick Southwick, Robert Cohen, and William Zeile for helpful discussions.

## REFERENCES

Angelastro, J. M., and D. L. Purich. 1994. Phosphorylation states of actin filament adenine nucleotides in detergent-extracted neuronal cytoskeletal fractions. *Biochem. Biophys. Res. Commun.* 201:1490–1494.

Bachmann, C., L. Fischer, U. Walter, and M. Reinhard. 1999. The EVH2 domain of the vasodilator-stimulated phosphoprotein mediates tetramerization, F-actin binding, and actin bundle formation. *J. Biol. Chem.* 274:23549–23557.

Bloom, L. B., J. Turner, Z. Kelman, J. M. Beechem, M. O'Donnell, and M. F. Goodman. 1996. Dynamics of loading the beta sliding clamp of DNA polymerase III onto DNA. *J. Biol. Chem.* 271:30699–30708.

Bray, D. 1992. Cell Movements. Garland Publishing, Inc., New York.

Cooke, R. 1975a. The bound nucleotide of actin. *J. Supramol. Struct.* 3:146–153.

Cooke, R. 1975b. The role of the bound nucleotide in the polymerization of actin. *Biochemistry.* 14:3250–3256.

Dabiri, G. A., J. M. Sanger, D. A. Portnoy, and F. S. Southwick. 1990. *Listeria monocytogenes* moves rapidly through the host-cell cytoplasm by inducing directional actin assembly. *Proc. Natl. Acad. Sci. U.S.A.* 87:6068–6072.

Doi, M., and S. F. Edwards. 1986. The Theory of Polymer Dynamics. Clarendon Press, Oxford, U.K.

Frischknecht, F., V. Moreau, S. Rottger, S. Gonfloni, I. Reckmann, G. Superti-Furga, and M. Way. 1999. Actin-based motility of vaccinia virus mimics receptor tyrosine kinase signalling. *Nature.* 401:926–929.

Gardiner, C. W. 1985. Handbook of Stochastic Methods for Physics, Chemistry, and the Natural Sciences. Springer-Verlag, New York.

Gertler, F. B., A. R. Comer, J. L. Juang, S. M. Ahern, M. J. Clark, E. C. Liebl, and F. M. Hoffmann. 1995. Enabled, a dosage-sensitive suppressor of mutations in the *Drosophila* Abl tyrosine kinase, encodes an Abl substrate with SH3 domain-binding properties. *Genes Dev.* 9:521–533.

Gittes, F., B. Mickey, J. Nettleton, and J. Howard. 1993. Flexural rigidity of microtubules and actin filaments measured from thermal fluctuations in shape. *J. Cell. Biol.* 120:923–934.

Götter, R., K. Kroy, E. Frey, M. Bärmmann, and E. Sackmann. 1996. Dynamic light scattering from semidilute actin solutions: a study of hydrodynamic screening, filament bending stiffness, and the effect of tropomyosin/troponin-binding. *Macromolecules.* 29:30–36.

Hajkova, L., T. Nyman, U. Lindberg, and R. Karlsson. 2000. Effects of cross-linked profilin:β/γ-actin on the dynamics of the microfilament system in cultured cells. *Exp. Cell Res.* 256:112–121.

Higuchi, H., T. Yanagida, and Y. E. Goldman. 1995. Compliance of thin filaments in skinned fibers of rabbit skeletal muscle. *Biophys. J.* 69: 1000–1010.

Isambert, H., and A. Maggs. 1996. Dynamics and rheology of actin solutions. *Macromolecule.* 29:1036–1040.

Janmey, P. A., S. Hvidt, G. F. Oster, J. Lamb, T. P. Stossel, and J. H. Hartwig. 1990. Effect of ATP on actin filament stiffness. *Nature*. 347: 95–99.

Karr, T. L., A. E. Podrasky, and D. L. Purich. 1979. Participation of guanine nucleotides in nucleation and elongation steps of microtubule assembly. *Proc. Natl. Acad. Sci. U.S.A.* 76:5475–5479.

Khan, S., and M. P. Sheetz. 1997. Force effects on biochemical kinetics. *Annu. Rev. Biochem.* 66:785–805.

Kuo, S. C., and J. L. McGrath. 2000. Steps and fluctuations of *Listeria monocytogenes* during actin-based motility. *Nature.* 407:1026–1029.

Kuriyan, J., and M. O'Donnell. 1993. Sliding clamps of DNA polymerases. *J. Mol. Biol.* 234:915–925.

Laine, R. O., W. Zeile, F. Kang, D. L. Purich, and F. S. Southwick. 1997. Vinculin proteolysis unmasks an ActA homolog for actin-based *Shigella* motility. *J. Cell Biol.* 138:1255–1264.

Lindberg, U., A. S. Höglund, and R. Karlsson. 1981. On the ultrastructural organization of the microfilament system and the possible role of profilactin. *Biochimie.* 63:307–323.

MacNeal, R. K., and D. L. Purich. 1978. Stoichiometry and role of GTP hydrolysis in bovine neurotubule assembly. *J. Biol. Chem.* 253: 4683–4687.

McClure, W. R., and Y. Chow. 1980. The kinetics and processivity of nucleic acid polymerases. *Methods Enzymol.* 64:277–297.

Merkel, R., P. Nassoy, A. Leung, K. Ritchie, and E. Evans. 1999. Energy landscapes of receptor–ligand bonds explored with dynamic force spectroscopy. *Nature.* 397:50–53.

Mimuro, H., T. Suzuki, S. Suetsugu, H. Miki, T. Takenawa, and C. Sasakawa. 2000. Profilin is required for sustaining efficient intra- and intercellular spreading of *Shigella flexneri*. *J. Biol. Chem.* 275: 28893–28901.

Mogilner, A., and G. Oster. 1996. Cell motility driven by actin polymerization. *Biophys. J.* 71:3030–3045.

Niebuhr, K., F. Ebel, R. Frank, M. Reinhard, E. Domann, U. D. Carl, U. Walter, F. B. Gertler, J. Wehland, and T. Chakraborty. 1997. A novel proline-rich motif present in ActA of *Listeria monocytogenes* and cytoskeletal proteins is the ligand for the EVH1 domain, a protein module present in the Ena/VASP family. *EMBO J.* 16:5433–5444.

Noireaux, V., R. M. Golsteyn, E. Friederich, J. Prost, C. Antony, D. Louvard, and C. Sykes. 2000. Growing an actin gel on spherical surfaces. *Biophys. J.* 78:1643–1654.

O'Brien, E. T., W. A. Voter, and H. P. Erickson. 1987. GTP hydrolysis during microtubule assembly. *Biochemistry.* 26:4148–4156.

Otterbein, L. R., P. Graceffa, and R. Dominguez. 2001. The crystal structure of uncomplexed actin in the ADP state. *Science.* 293:708–711.

Peskin, C. S., G. M. Odell, and G. F. Oster. 1993. Cellular motions and thermal fluctuations: the Brownian ratchet. *Biophys. J.* 65:316–324.

Pollard, T. D. 1986a. Assembly and dynamics of the actin filament system in nonmuscle cells. *J. Cell Biochem.* 31:87–95.

Pollard, T. D. 1986b. Rate constants for the reactions of ATP- and ADP-actin with the ends of actin filaments. *J. Cell Biol.* 103:2747–2754.

Pollard, T. D., L. Blanchoin, and R. D. Mullins. 2000. Molecular mechanisms controlling actin filament dynamics in nonmuscle cells. *Annu. Rev. Biophys. Biomol. Struct.* 29:545–576.

Purich, D. L. 2001. Enzyme catalysis: a new definition accounting for noncovalent substrate- and product-like states. *Trends Biochem. Sci.* 26:417–421.

Purich, D. L., and J. M. Angelastro. 1994. Microtubule dynamics: bioenergetics and control. *Adv. Enzymol. Relat. Areas Mol. Biol.* 69:121–154.

Purich, D. L., and F. S. Southwick. 1999. Energetics of nucleotide hydrolysis in polymer assembly/disassembly: the cases of actin and tubulin. *Methods Enzymol.* 308:93–111.

Rayment, I., C. Smith, and R. G. Yount. 1996. The active site of myosin. *Annu. Rev. Physiol.* 58:671–702.

Reinhard, M., T. Jarchau, and U. Walter. 2001. Actin-based motility: stop and go with Ena/VASP proteins. *Trends Biochem. Sci.* 26:243–249.

Scholey, J. M., M. E. Porter, P. M. Grissom, and J. R. McIntosh. 1985. Identification of kinesin in sea urchin eggs, and evidence for its localization in the mitotic spindle. *Nature.* 318:483–486.

Sechi, A. S., J. Wehland, and J. V. Small. 1997. The isolated comet tail pseudopodium of *Listeria monocytogenes*: a tail of two actin filament populations, long and axial and short and random. *J. Cell Biol.* 137: 155–167.

Southwick, F. S., and D. L. Purich. 1996. Intracellular pathogenesis of listeriosis. *N. Engl. J. Med.* 334:770–776.

Stossel, T. P. 1993. On the crawling of animal cells. *Science.* 260: 1086–1094.

Suzuki, T., S. Saga, and C. Sasakawa. 1996. Functional analysis of *Shigella* VirG domains essential for interaction with vinculin and actin-based motility. *J. Biol. Chem.* 271:21878–21885.

Vale, R. D. 1996. Switches, latches, and amplifiers: common themes of G proteins and molecular motors. *J. Cell Biol.* 135:291–302.

Wegner, A. 1982. Treadmilling of actin at physiological salt concentrations. An analysis of the critical concentrations of actin filaments. *J. Mol. Biol.* 161:607–615.

Wegner, A., and J. Engel. 1975. Kinetics of the cooperative association of actin to actin filaments. *Biophys. Chem.* 3:215–225.

Zeile, W. L., R. C. Condit, J. I. Lewis, D. L. Purich, and F. S. Southwick. 1998. Vaccinia locomotion in host cells: evidence for the universal involvement of actin-based motility sequences ABM-1 and ABM-2. *Proc. Natl. Acad. Sci. U.S.A.* 95:13917–13922.

Zeile, W. L., D. L. Purich, and F. S. Southwick. 1996. Recognition of two classes of oligoproline sequences in profilin-mediated acceleration of actin-based *Shigella* motility. *J. Cell Biol.* 133:49–59.